

Fast Prediction Method for Radial Growth of Labyrinth Seal Clearance Based on Transient Thermal-Fluid Coupling Network

Zijun Li¹, Chuankai Liu¹, Peng Liu¹, Yufei Wang¹, Xin Jin¹, Shuiting Ding¹

¹ Research Institute of Aero-Engine, Beihang University, Beijing, 102206, China

Abstract

The labyrinth seal clearance is an important geometric parameter that affects the labyrinth seals. Its reasonable design value is not only beneficial for improving the efficiency and stability of the engine, but also for enhancing the safety of the engine. However, the current analysis and prediction methods for the radial growth of the labyrinth seal clearance during the transition process are still constrained by computational power, and cannot quickly evaluate the radial clearance deformation of the labyrinth seal during the transition process. This paper proposed a transient secondary air system thermal-fluid-structure coupling fast prediction model, which reduced the dimensionality of the high-dimensional solid model on the basis of the transient thermal-fluid coupling network model. Therefore, the model had the ability to quickly predict the radial growth of the labyrinth seal clearance during the transition process, and a thermal-fluid-structure coupling test platform for labyrinth seals was established in a laboratory environment for experimental verification. The verification results showed that the fast prediction model ensures an accuracy of predicting radial growth of the labyrinth seal clearance during the transition process within 10% (maximum relative error is 8.54%). The simulation time is shortened to about 8 minutes.

Keywords: Labyrinth seals; thermal-fluid-structure coupling; Transient Process; Experimental verification

1. Introduction

The labyrinth seal is a typical rotary static seal element. It is widely used in the secondary air system of aero engines due to its good stability and high reliability. The seal clearance is the most critical geometric parameter affecting the performance of labyrinth seals. Excessive seal clearance can lead to a decrease in engine efficiency and aerodynamic stability, while too small seal clearance can increase the risk of friction between the rotor and stator and reduce engine safety. During the actual operation of the engine, the labyrinth seal clearance is in a complex environment with changing boundary conditions. It is constantly affected by changing aerodynamic loads, centrifugal loads, and thermal loads, resulting in the actual seal clearance value of the labyrinth seal also changing. In recent years, there have been multiple failures such as in-flight Shutdown, rotor Clamping fault, and seal ring fractured caused by deviation in the seal clearance, which have seriously endangered the normal and safe operation of aero engines[1]-[2]. Therefore, during the engine design phase or real-time prediction environment, as the performance requirements and structural complexity of the engine gradually increase, it is increasingly necessary to have the ability to quickly evaluate and predict the radial growth of the labyrinth seal clearance during the transition process.

As the most important geometric parameter affecting the sealing performance of the labyrinth seals, seal clearance has been studied by many researchers on the impact of changes in seal clearance on their performance. Among them, Subramanian S et al. [3]-[6] used finite element commercial software and analytical algorithms to decouple and calculate the centrifugal deformation and thermal deformation of labyrinth seals, and analyzed the contribution of centrifugal deformation

and thermal deformation to the deformation of the labyrinth clearance; Kong et al. [7]-[9] analyzed the effects of different clearances, teeth numbers, and rotational speeds on the leakage performance of labyrinth seals in compressor stages. They conducted experimental verification in a laboratory environment and found that the seal clearance has a significant impact on the leakage flow rate.

However, it is difficult to accurately provide the simulation boundary for the deformation analysis of labyrinth seals in the engine environment. Therefore, the above researches mainly focused on the leakage characteristics of a single labyrinth seal element under steady-state conditions.

To solve the problem of insufficient boundary accuracy in the deformation analysis of labyrinth seals, researchers used the full three-dimensional thermal-fluid-structure coupling solution method to analyze the mass flow, heat transfer, thermal conductivity, and deformation characteristics. Valencia A G et al. [10] considered the thermal (working) clearance of the labyrinth seal and established a coupled simulation of turbine hub cavities combining CFD and FE. However, it took 3-4 days for them to simulate a steady-state point calculation; Lück et al. [11] used implicit MFX coupling and explicit manual coupling method respectively to analyze the transient thermal-fluidstructure coupling of labyrinth seal clearance. They found that explicit manual coupling method is more effective, and also demonstrated that there is not much difference between 2D model and 3D model. Therefore, 2D model can be used to replace 3D model for simulation acceleration. Amirante et al. [12]-[14]proposed a mesh deformation method suitable for transient thermal-fluid-structure coupling calculation based on the analogy method of elastic media, which was applied to the analysis of labyrinth seal clearance in turbine stages. This type of method has high solving accuracy, but it has not been widely used in the industry. The reason is that full 3D simulation requires extremely high computing power, with a computing speed of over 10¹² times per second, and requires a considerable amount of computing and time resources;

Thus, some researchers, to reduce computational costs, use low-dimensional fluid network models instead of high-dimensional fluid calculation models to achieve multi-dimensional and multi-physical field coupling analysis of the labyrinth seal clearance. Tondello et al. [15] established a low-dimensional fluid network model and a high-dimensional thermal structural analysis model for steady-state labyrinth seal clearance analysis of typical secondary air systems. Ganine et al. [16] established a multidimensional and multi-physics field coupling model, and conducted transient calculations on the labyrinth seal, obtaining the variation of the seal clearance during the acceleration process. Giuntini et al. [17] conducted secondary development based on the CalculiX program and analyzed the transient thermal-fluid-structure coupling of an acceleration and a deceleration process, obtaining the deformation of four labyrinth seal clearances during the transition process. However, even if a multi-dimensional and multi-physics field coupling analysis model is used, it still requires a long calculation time and cannot meet the demand for fast prediction of radial growth deformation of labyrinth seals during the transition process in the design process, it is also impossible to achieve the real-time prediction of aero engine state during the transition process.

In conclusion, the current main methods for studying the radial growth of labyrinth seal clearance during the transition process have the problem of long calculation time. The main reason is that the current research methods require the establishment of three-dimensional/two-dimensional models of labyrinth seals and related solid geometry, which requires considerable amounts of computational resources and time in the calculation process. In response to the above issues, this paper has reduced the dimensionality of high-dimensional solid models and formed a transient secondary air system thermal-fluid-structure coupling fast prediction model. This model further reduces calculation time while ensuring calculation accuracy.

2. Method

On the basis of the transient thermal-fluid coupling network model formed by coupling the transient fluid network and the solid thermal network, this paper establishes a radial growth prediction module, as shown in Figure 1, to form the transient secondary air system thermal-fluid-structure coupling fast prediction model. This model considers energy conservation and mass flow conservation. Once the transient process of the secondary air system occurs in the model, which deviates from the design point of the calculation model, the following calculations are performed at

each time step: Firstly, the fast prediction model calculates the mass flow rate of each fluid element due to pressure imbalance; Secondly, based on the heat transfer process occurring at different elements, the fast prediction model uses empirical heat transfer formulas to calculate the air temperature and solid temperature; Then, the fast prediction model calculates the rotor deformation based on the rotor temperature distribution and rotational speed of the labyrinth seal disk, and calculates the stator deformation based on the temperature of the stator and the pressure of the inner and outer rings, obtaining the deformation in the labyrinth seal clearance at the current time step; Finally, the fast prediction model transfers the deformation of the labyrinth seal clearance to the corresponding labyrinth seal element, starting a new iteration at the current time step until convergence.

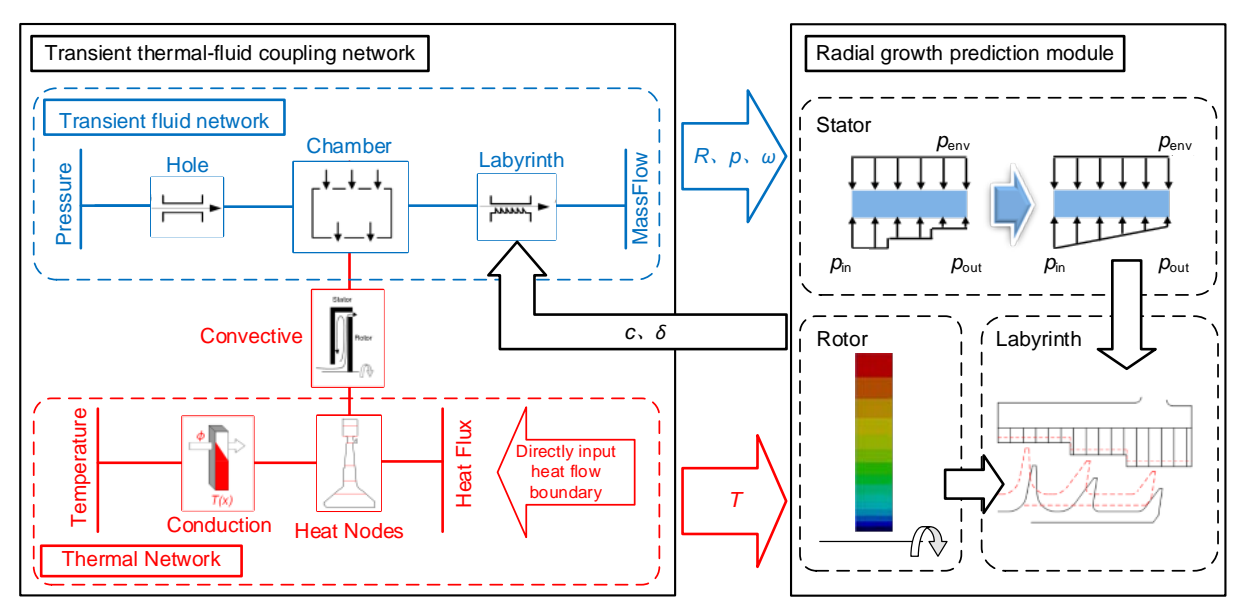


Figure 1 - Schematic of Fast prediction model diagram

2.1 Thermal-fluid coupling network

the transient thermal-fluid coupling network model contains two parts: the transient fluid network and the solid thermal network. The transient fluid network is used to calculate the flow parameters of each flow path in the secondary air system, including mass flow rate, gas pressure, and gas temperature. The solid thermal network calculates the solid temperature through convective heat transfer components and solid conduction components. The mathematical models of various components will be introduced in the following sections.

2.1.1 The transient fluid network

The transient fluid network is used to model the engine secondary air system. The transient fluid network abstracts the secondary air system as chamber elements and flow resistance elements (Including hole, gap and labyrinth seal, and other elements), which are connected to each other to form a fluid network. The chamber element considers transient volume effect and gas inertia, while the other flow resistance elements are connected between the chamber elements.

Modelling of the chamber element

The chamber element is considered to be a larger volume cavity structure within the secondary air system (considered as a node in steady-state calculations), satisfying the following assumptions in the model [18]:

- The gas velocity inside the chamber element is low enough to ignore the difference in total/static parameters inside the chamber element;
- The inlet area of each branch is much smaller than the surface area of the chamber;
- The chamber element adopts a lumped assumption, which means that the internal flow parameters are only related to time and not to space;

Based on the above assumptions, the transient fluid network establishes a schematic of the

chamber element as shown in Figure 2. Where $W_{v,i}$ is the mass flow of the i-th path, $Q_{v,j}$ is the heat flow of the j-th heat transfer zone connected to the chamber, A_v is the inlet/outlet area, p_v is the air static pressure, p_v^* is the air total pressure, T_v is the air static temperature, T_v^* is the air total temperature, ω is the angular velocity. In the chamber element, calculate the gas density ρ_v according to the following equation:

$$\rho_{v} = \frac{\rho_{v}^{*}}{RT_{v}^{*}} \tag{1}$$

Where, R is the gas constant.

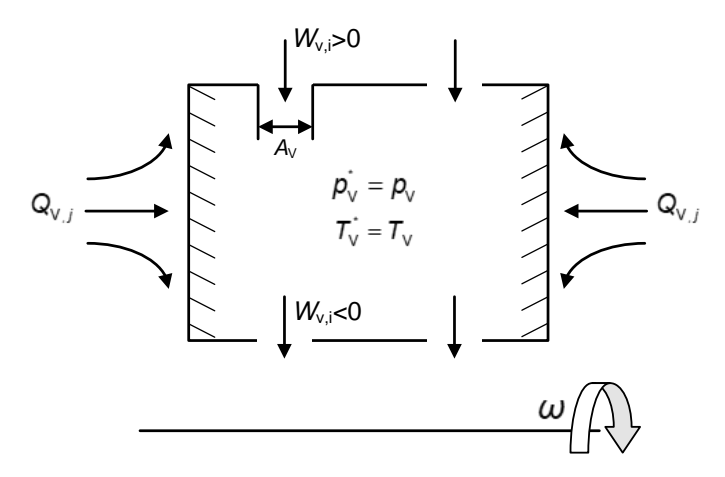


Figure 2 – Schematic of the chamber element

The transient fluid network considers the secondary air system as composed of multiple flow resistance elements and cavity elements connected. Assuming the number of flow paths (branches) connected to the cavity element is M and the number of convective heat transfer zones is N, the mass flow continuity equation and energy conservation equation of the cavity element are established as follows:

$$V\frac{\mathrm{d}\rho_{\mathrm{v}}}{\mathrm{d}t} = \sum_{i=1}^{M} W_{\mathrm{v},i} \tag{2}$$

$$V\frac{d(\rho_{v}e_{v})}{dt} = \sum_{i=1}^{M} W_{v,i} h_{v,i}^{*} + \sum_{j=1}^{N} Q_{v,j} + P_{win}$$
(3)

Where, V is the volume of the chamber, e_V is the specific internal energy of the air inside the chamber, $h_{V,i}^*$ is the specific enthalpy of the the i-th path, t is the time, P_{Win} is the windage power, and for a stationary chamber, $P_{Win} = 0$.

Modelling of the labyrinth seal element

The schematic of the straight labyrinth seal is shown in Figure 3, where c represents the seal clearance, r_{lab} represents the radius of the labyrinth seal.

The labyrinth seal element adopts the classic labyrinth sealing leakage equation to model the flow characteristics of the labyrinth, as follows [19]:

$$W_{\text{lab}} = \sqrt{\frac{\left(p_{\text{lab,in}}^{*}^{2} - p_{\text{lab,out}}^{*}^{2}\right)B^{2}A_{\text{lab}}^{2}}{nRT_{\text{in}}^{*}}}$$
(4)

$$A_{\rm ab} = 2\pi r_{\rm lab} c \tag{5}$$

$$c = c_0 + \delta \tag{6}$$

Where, W_{lab} is the mass flow of the labyrinth, $p_{lab,in}^*$ and $p_{lab,out}^*$ are the total inlet pressure and outlet pressure of the labyrinth, B is the empirical coefficient of the labyrinth, A_{lab} is the annular area

between the labyrinth tip and the stator. n is the number of teeth of the labyrinth, $T_{\rm in}^*$ is the total inlet temperature of the labyrinth, π is the ratio of circumference to diameter, c_0 is the initial seal clearance, and δ is the deviation value of the clearance during the transition process.

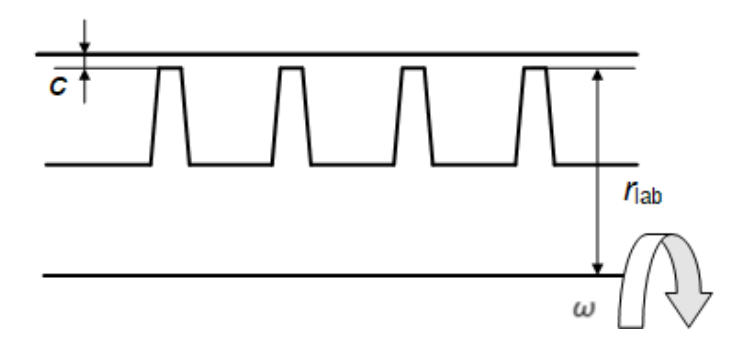


Figure 3 - Schematic of the straight labyrinth seal

The clearance deviation value δ includes two parts: the rotor deviation value and the stator deviation value. The deviation values are obtained by the radial growth prediction module. In this calculation, it is considered that the rotor radius is lower than the stator radius. Therefore, the deviation calculation is as follows:

$$\delta = \delta_{s} - \delta_{r} \tag{7}$$

Where, δ_s is the stator deviation value, δ_r is the rotor deviation value.

2.1.2 The solid thermal network

The thermal network model includes solid thermal nodes and solid thermal conductivity. The thermal conduction between solid thermal nodes is described by Fourier's law of thermal conductivity, forming a thermal conductivity resistance element. The Newton's law of cooling is used to describe the convective heat transfer between fluid networks and thermal networks, where the convective heat transfer coefficient *H* is calculated using an empirical equation based on the geometric characteristics and flow characteristics of the actual model.

2.2 Radial growth prediction module

The radial growth prediction module receives parameters such as fluid pressure, solid temperature, and rotational speed transmitted from the transient thermal-fluid coupling network model. The stator is mainly affected by thermal and aerodynamic loads. The structure of the stator is relatively simple, ignoring the temperature changes of the stator. The internal pressure of the stator is distributed in a stepped manner due to the influence of the labyrinth structure. It is equivalent to a linear distribution, as shown in the Figure 1. Based on the stress and strain calculation equation in elastic mechanics [20], a deformation displacement equation for the stator caused by thermal and aerodynamic loads is established as follows:

$$u_{\rm s1} = \alpha_{\rm s} r_{\rm s,in} T_{\rm s} \tag{8}$$

$$u_{s2} = \frac{1}{E_{s}(r_{s,out}^{2} - r_{s,in}^{2})} [(1 - v_{s}) r_{s,in} (p_{in} r_{s,in}^{2} - p_{out} r_{s,out}^{2}) - (1 + v_{s}) r_{s,in} r_{s,out}^{2} (p_{out} - p_{in})]$$
(9)

Where, $u_{\rm s1}$ and $u_{\rm s2}$ are the deformations caused by thermal and aerodynamic loads on the stator, $\alpha_{\rm s}$, $E_{\rm s}$ and $V_{\rm s}$ are the linear expansion coefficient, elastic modulus, and Poisson's ratio of the stator material, $r_{\rm s,in}$ and $r_{\rm s,out}$ are the inner and outer radius of the stator, $T_{\rm s}$ is the temperature of the stator, $p_{\rm in}$ and $p_{\rm out}$ are total pressures at the inlet and outlet of labyrinth.

In this module, the rotor structure is considered as a hollow equally thick rotating disk as shown in Figure 4. The cooling flow path passing through the disk center usually has a lower temperature, while the labyrinth seal located at the high radius of the rotor is exposed in the core flow path with higher temperature. Therefore, the following assumptions are made regarding the structure of the

rotor disk:

- The rotor only considers the thermal and centrifugal deformation caused by thermal and centrifugal loads, ignoring the deformation caused by rotor vibration;
- The rotor only considers the influence of the non-uniformity of temperature distribution along the radial direction on the clearance, ignoring the influence of the non-uniformity of temperature distribution along the axial direction;

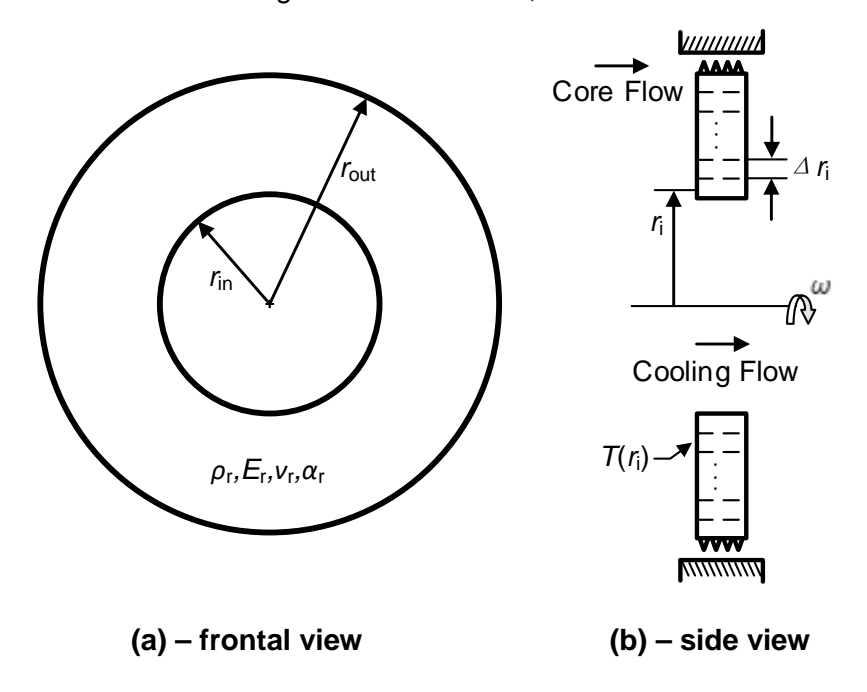


Figure 4 – Schematic of Rotor

During engine operation, the non-uniformity of temperature distribution along the radial direction of the rotor disk is significant and cannot be ignored. Therefore, the rotor disk is divided into multiple lumped solid thermal nodes along the radial direction, and the calculated values of each thermal node are used to represent the equivalent temperature of each part, as shown in Figure 4 (b). According to the theory of elasticity [20], the calculation formulas for discrete thermal deformation and centrifugal deformation of rotor components are constructed as follows:

$$u_{r1} = \frac{1 + v_r}{1 - v_r} \frac{\alpha_r}{r_{rout}} \left[\sum_{i=1}^n T(r_i) r_i \Delta r_i + \left(r_{r,in}^2 + \frac{1 - 3v_r}{1 + v_r} r_{r,out}^2 \right) \frac{1}{r_{rout}^2 - r_{r,in}^2} \sum_{i=1}^n T(r_i) r_i \Delta r_i \right]$$
(10)

$$u_{r2} = \frac{1}{4E_{r}} (1 - v_{r}) \rho_{r} \omega^{2} r_{r,out}^{3}$$
 (11)

Where, u_{r1} and u_{r2} are the deformations caused by thermal and mechanical loads on the rotor, ρ_r , α_r , E_r and V_r are the density, linear expansion coefficient, elastic modulus, and Poisson's ratio of the stator material, $r_{r,in}$ and $r_{r,out}$ are the inner and outer radius of the rotor, r_i is the radial position of the i-th thermal node, $T(r_i)$ is the solid temperature at the i-th thermal node, Δr_i is the radial division length of the i-th thermal node.

Based on the actual assembly position of the rotor and stator (usually the rotor radius is lower than the stator radius), the radial growth prediction module calculates the actual transition process labyrinth seal clearance (see equation 12-14), and transmits it to the labyrinth seal element to achieve fast prediction of the radial growth of seal clearance during the transition process:

$$\delta_{s} = U_{s1} + U_{s2} \tag{12}$$

$$\delta_{r} = u_{r1} + u_{r2} \tag{13}$$

$$\delta = U_{s1} + U_{s2} - U_{r1} - U_{r2} \tag{14}$$

3. Experiment & Simulation

3.1 Experimental system

Figure 5 shows the overall layout of the experimental system, which consisted of a supply and exhaust component, a gas heating component, a rotating mechanical drive component, a console component, and a data acquisition component. Three screw compressors could provide a maximum continuous flow rate of 2.0kg/s at a pressure of 0.8Mpa. The experimental system heated the rotor disk to change the labyrinth seal clearance. The experimental system was equipped with a 60kw heater, with a maximum operating temperature of 500K.

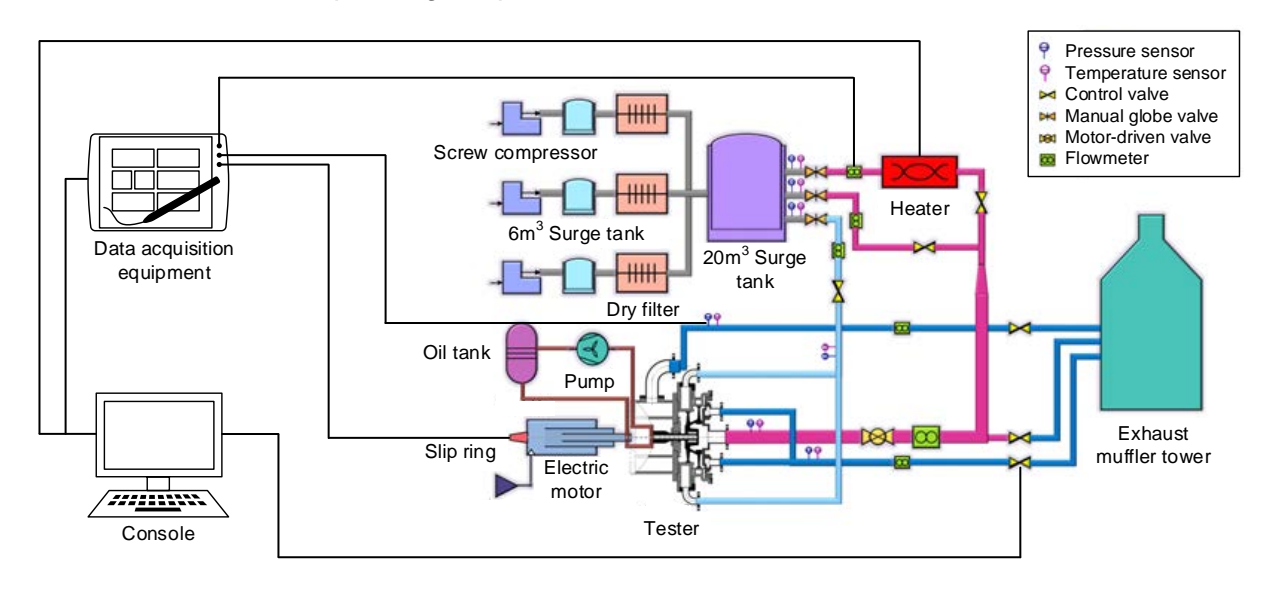


Figure 5 - Schematic of experimental system

3.2 Test rig

This paper established a thermal-fluid-structure coupling test rig for labyrinth seals that can provide analogous criteria boundaries during the aero engine transition process in a laboratory environment. This experimental platform adopted a two-in two-out flow design scheme, as shown in the Figure 6.

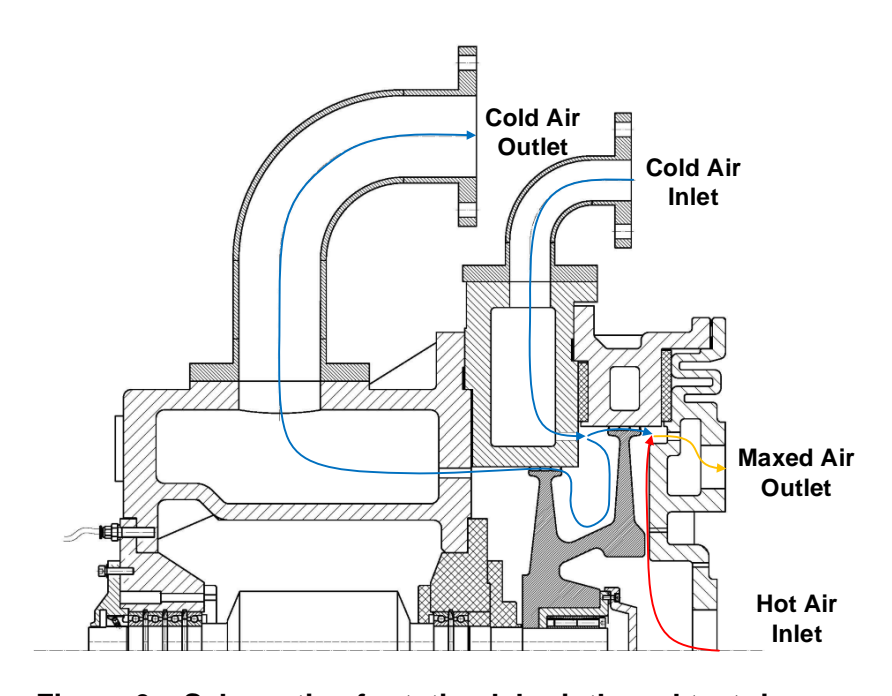


Figure 6 – Schematic of rotating labyrinth seal test rig

The experiment adjusted non-dimensional parameters such as rotational Reynolds number, flow

coefficient, and non-dimensional maximum temperature difference by controlling the motor speed, air supply valve opening degree, and electric heater temperature. The rotor adopted a double disk structure, with a balance disk on the left for balancing axial force and a coupling disk on the right for experimental verification. The stator was equipped with pressure, temperature, and displacement sensors, and a circulating water chamber was designed to suppress the deformation of the stator caused by hot air heating to control the heating effect of the hot air only on the rotor.

3.3 Clearance measurement

The measurement of labyrinth seal clearance was a core part of this experiment, which adopted a combination of static and dynamic testing method to obtain the labyrinth seal clearance during the transition process. In the stationary state, a feeler gauge was used to measure 12 uniformly selected positions in the circumferential direction (every 30 °) for testing, and the measurement was repeated multiple times to obtain the circumferential distribution of the labyrinth seal clearance in the initial state, as shown in Figure 7. The average value of 0.81mm was taken as the initial clearance value.

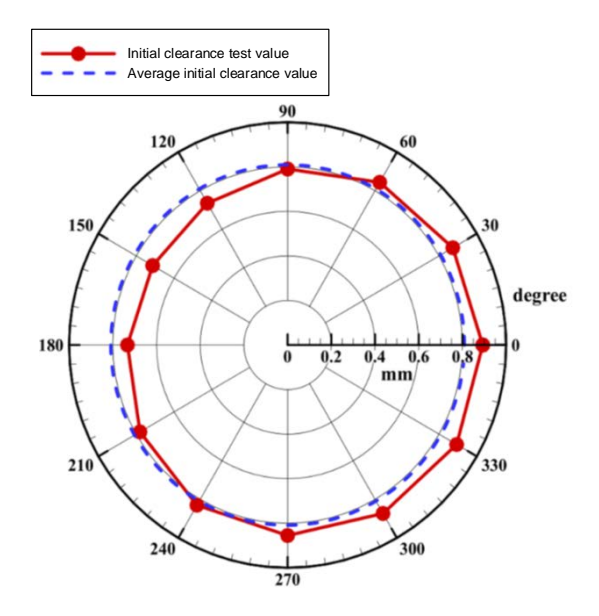


Figure 7 - Static test location and measurement results

In the rotating state, laser distance sensors were used to measure the deformation value of the rotor, and contact distance sensors were used to measure the deformation value of the stator, as shown in Figure 8 Therefore, the clearance measurement of the labyrinth seal during the transition process is as follow:

$$c_{\text{exp}} = c_{\text{exp,0}} - \Delta c_{\text{exp,r}} + \Delta c_{\text{exp,s}}$$
 (15)

Where, $c_{\rm exp}$ is the clearance measurement value, $c_{\rm exp,0}$ is the initial clearance measurement value, $\Delta c_{\rm exp,r}$ is the rotor deformation measurement value, $\Delta c_{\rm exp,s}$ is the stator deformation measurement value.

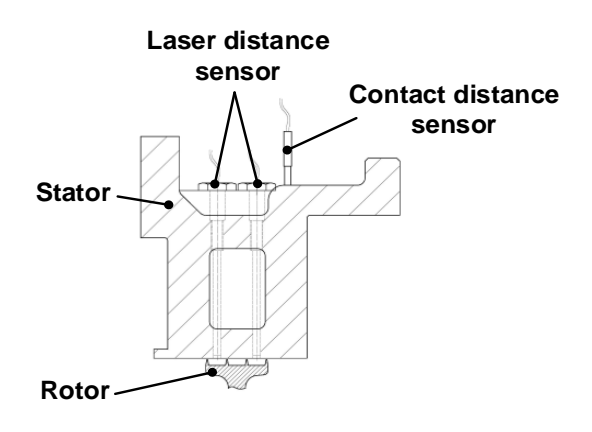
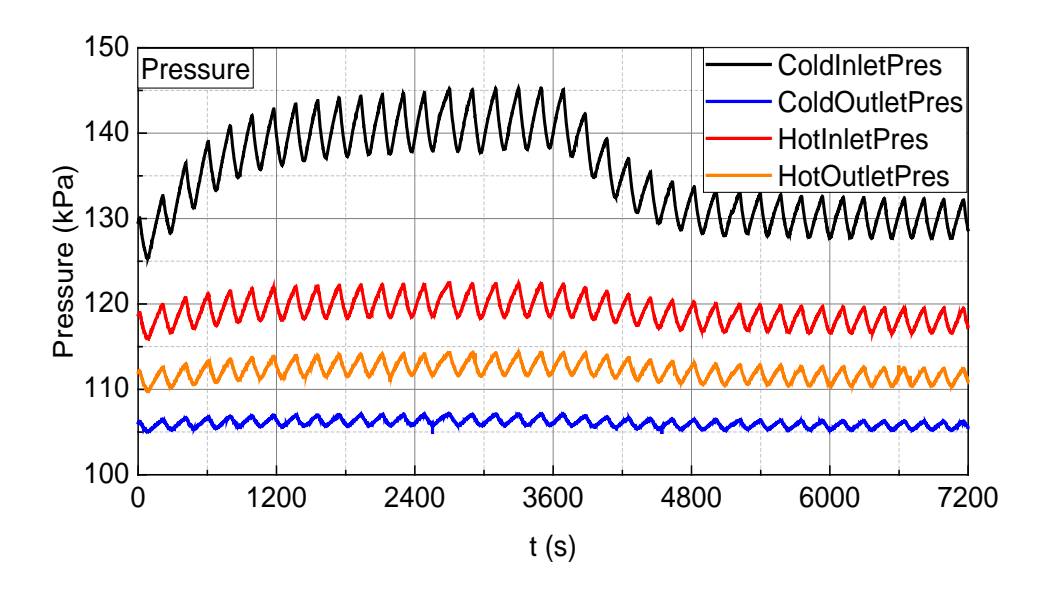


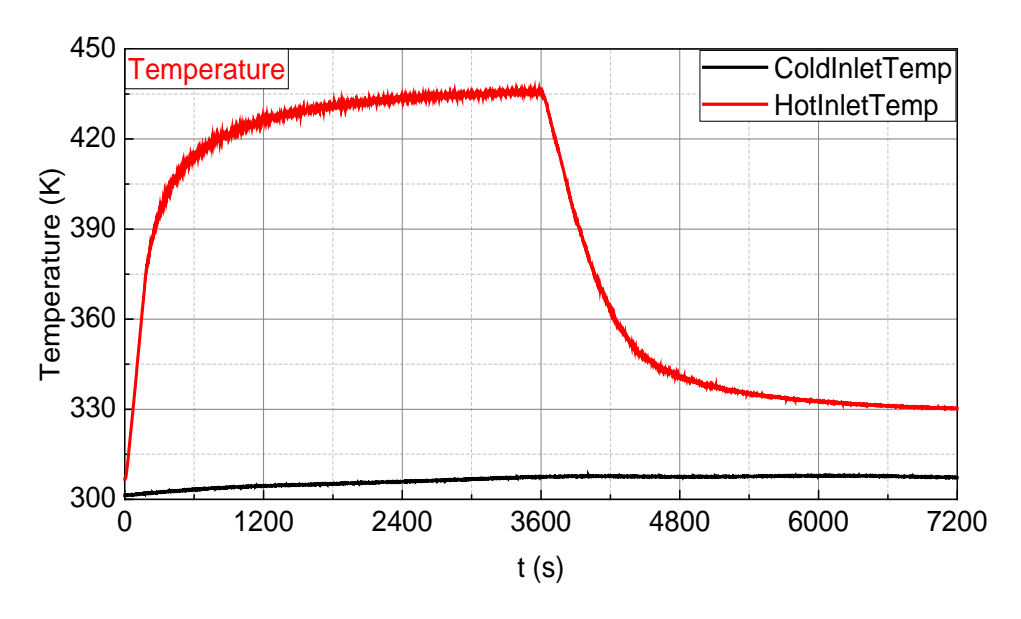
Figure 8 - Installation diagram of two types distance sensors

3.4 Test boundary

According to the working state of typical labyrinth seal structures in aero engines, the test inlet/outlet pressure and temperature boundaries are shown in Figure 9. During the experiment, the first 3600s was the heating stage of the experiment. The heater was turned on, and the inlet temperature of the hot gas branch rose, increasing the radial deformation of the rotor disk; The last 3600s was the cooling stage of the experiment. The heater was turned off, and the inlet temperature of the hot gas branch decreased, reducing the radial deformation of the rotor disk.



(a) Test pressure boundary



(b) Test temperature boundary

Figure 9 - Test pressure and temperature boundary

3.5 Simulation model

3.5.1 Rotor thermal network model

The experiment used the method of heating the rotor disk to generate radial deformation of the labyrinth seal. Therefore, the model needed to simulate the temperature of the labyrinth disk precisely in order to accurately predict the evolution of the clearance during the transition process. The rotor thermal network model divided the heat transfer zones and established heat nodes based on the actual arrangement of temperature sensors, as shown in Figure 10.

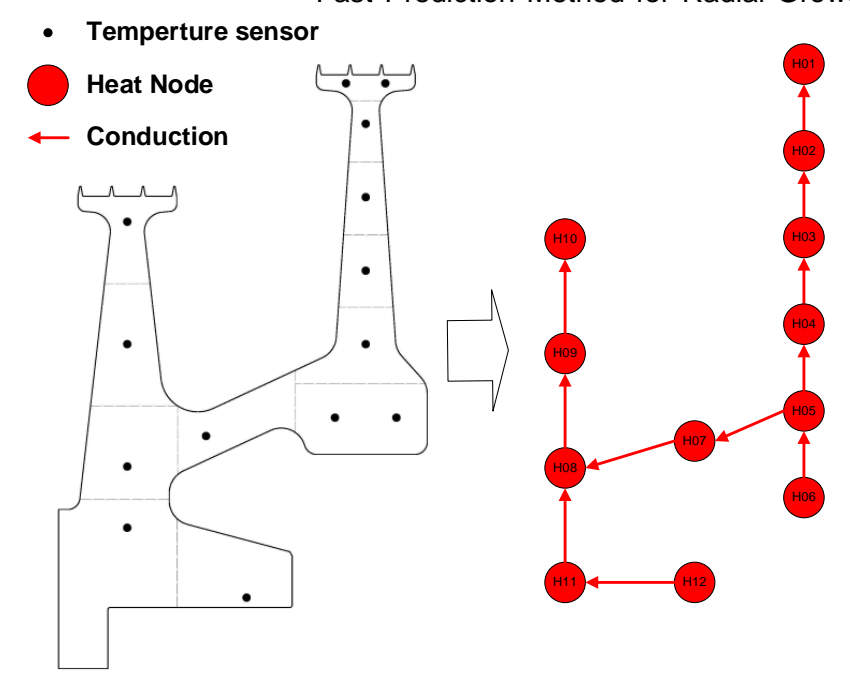


Figure 10 – Schematic of rotor thermal network model

3.5.2 Transient fluid network of test

The transient fluid network model also adopted a lumped partitioning method to establish corresponding chamber nodes and flow resistance elements based on the actual experimental environment chamber structure, as shown in Figure 11.

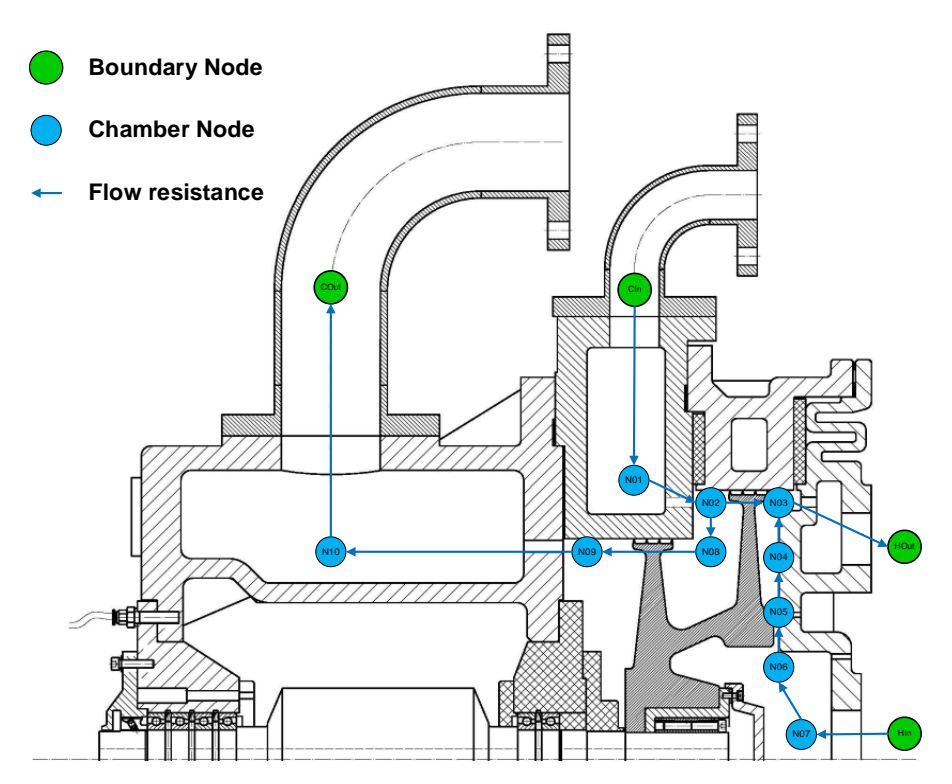


Figure 11 - Schematic of transient fluid model for test

4. Result

Based on the fast prediction method, a low dimensional transient secondary air system thermal-fluid-structure coupling fast prediction model for the laboratory environment was established. The model boundary was consistent with the actual experimental data, and predicted the radial growth of typical labyrinth seal structures. The simulation time for the transition process was about 8 minutes

(about 463 seconds).

4.1 Rotor temperature results

The main analysis target is the rotor disk on the right side of the test rig, and the solid thermal node corresponding to the simulation model is H01-H06, as shown in Figure 10. During the heating process, as the hot gas temperature rapidly rose, the temperature of the rotor disk also rose, showing a trend of rapid temperature rise in the beginning and then gradually flattening; During the cooling process, the rotor temperature also showed a trend of rapidly decreasing in the beginning and then gradually decreasing slowly. The reason for the above trends is that at the initial stage of temperature heating or cooling, there was a significant temperature difference between the rotor disk and the surrounding gas, resulting in a rapid temperature change stage caused by strong convective heat transfer. When the rotor disk temperature gradually approached the temperature of the surrounding gas, it entered the stage of slow temperature change. During the simulation process, the temperature predictions for each zone of the right rotor disk were in good agreement with the experimental measurements, with a maximum absolute error of 4.26K, as shown in Figure 12.

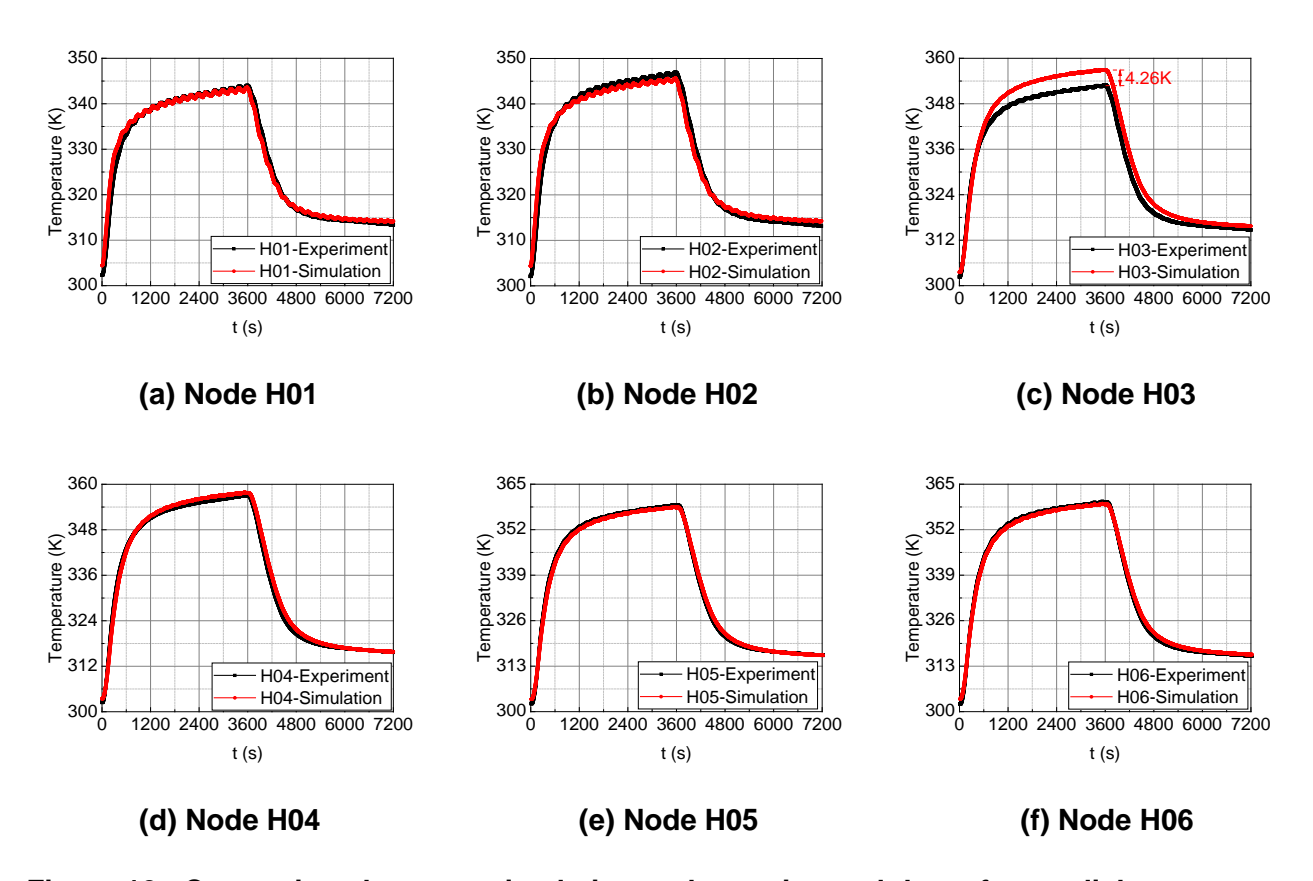


Figure 12 - Comparison between simulation and experimental data of rotor disk temperature

4.2 Labyrinth seal clearance results

As shown in Figure 13, the simulation values of the labyrinth seal clearance were consistent with the experimental data trend, except a certain error with a maximum relative error of 8.54%. The variation of labyrinth seal clearance was composed of stator deformation and rotor deformation. In this experiment, the stator deformation was much smaller than the rotor deformation due to the cooling water. Therefore, the deformation of labyrinth seal clearance is mainly affected by the thermal deformation of the rotor. In the heating section, the seal clearance gradually decreased, while in the cooling section, the seal clearance gradually increased. Similar to the temperature change trend of the rotor disk, the labyrinth seal clearance also has two parts of rapid deformation process and slow deformation process. However, the simulation values of the radial temperature distribution of the rotor disk were in good agreement with the experimental data. Therefore, it is considered that the source of the error is the deformation error caused by the non-uniformity of the axial temperature distribution of the rotor disk.

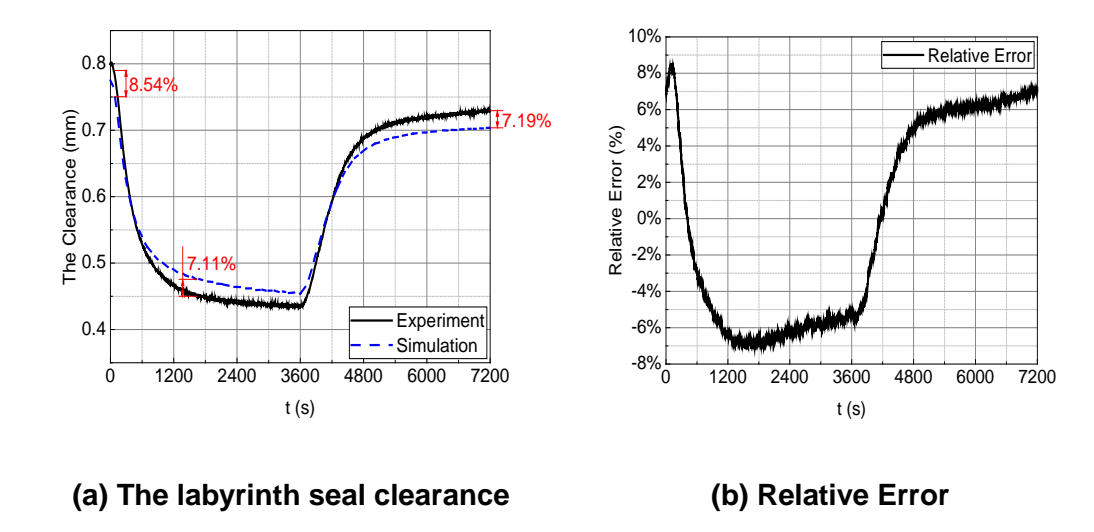


Figure 13 - Comparison between simulation and experimental data of labyrinth seal clearance

4.3 Fluid pressure and temperature results

The labyrinth seal clearance had a significant impact on the front and rear chambers, as shown in Figure 13, corresponding to N02 and N03 of the simulation model. During the experiment, due to the continuous influence of hot gas temperature on the right rotor disk, the labyrinth seal clearance constantly changed, resulting in constant changes in the pressure and temperature of the front chamber of the labyrinth seal, as shown in Figure 14.

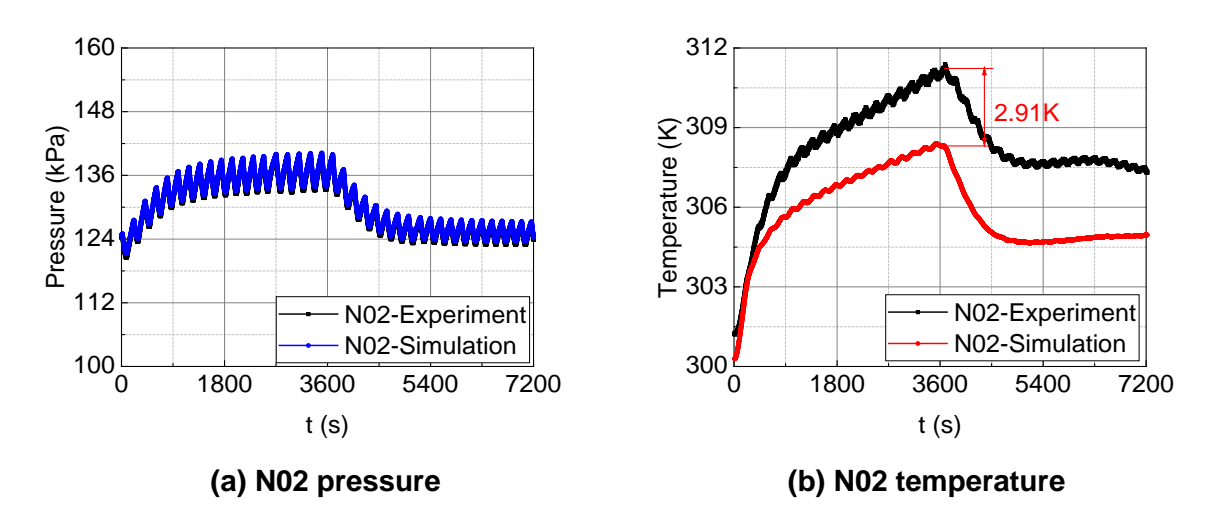


Figure 14 - Comparison between simulation and experimental data of front chamber (N02)

Figure 14 (a) and (b) represent the pressure and temperature in the front chamber of the labyrinth seal, respectively. During the heating process, the labyrinth seal clearance downstream of the chamber continuously decreased, and the chamber pressure and temperature gradually increased; During the cooling process, there was a trend of gradually decreasing of chamber pressure and temperature. The simulation and experimental data of the pressure in the chamber were in good agreement, and the periodic fluctuations in the chamber are mainly affected by the upstream gas source; The simulation of chamber temperature and experimental data showed a consistent trend with time, except a maximum absolute error of 2.91K. This is because the assumption of the stator component as a hot node in the calculation process ignored the temperature gradient of the stator. The calculated temperature of the stator was lower than the actual measured temperature, increasing the heat transfer temperature difference, resulting in lower calculated chamber temperature than the experimental data.

Figure 15 (a) and (b) represent the pressure and temperature of the chamber after the labyrinth seal, respectively. During the heating stage, the upstream labyrinth seal clearance continuously decreased, and the upstream pressure continuously increased, leading to a gradual increase in the temperature and pressure of the downstream chamber; The cooling process also showed a gradual decrease in chamber pressure and temperature. However, there was an absolute error of 2.3 kPa between the simulated chamber pressure value and the experimental data. This is because the simulated value of the labyrinth seal clearance deformation is lower than the experimental data, so the simulated chamber pressure is slightly higher than the experimental data. The calculated temperature of the rear chamber is in good agreement with the actual measurement value, and the maximum absolute error is 2.47 K.

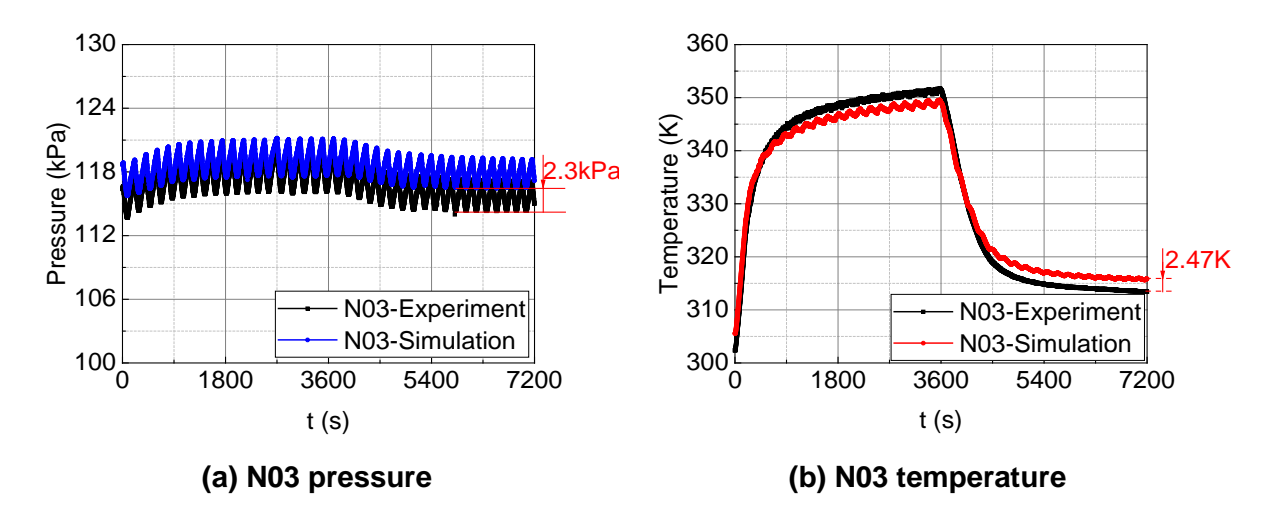


Figure 15 - Comparison between simulation and experimental data of rear chamber (N03)

5. Conclusion

This paper established the transient secondary air system thermal-fluid-structure coupling fast prediction model and compared it with experimental data for verification. The fast prediction model used experimental inlet/outlet temperature and pressure as simulation boundary conditions, and simulated the radial deformation process of the 7200s labyrinth seal clearance in a laboratory environment. The simulation time was only about eight minutes (about 463 seconds); By comparing the fast prediction model with experimental measurement data, the maximum relative deformation error of the labyrinth seal clearance was 8.54%; And it was found that the prediction of solid temperature and chamber temperature and pressure before and after labyrinth seal clearance was in good agreement. The maximum absolute error of solid temperature prediction was 4.26 K, the maximum absolute error of fluid pressure prediction was 2.3 kPa, and the maximum absolute error of fluid temperature prediction was 2.47 K. On the whole, the transient secondary air system thermal-fluid-structure coupling fast prediction model adopted in this paper greatly reduces simulation calculation time while ensuring high accuracy in predicting radial clearance growth of labyrinth seals.

6. Copyright Statement

The authors confirm that they, and/or their company or organization, hold copyright on all of the original material included in this paper. The authors also confirm that they have obtained permission, from the copyright holder of any third party material included in this paper, to publish it as part of their paper. The authors confirm that they give permission, or have obtained permission from the copyright holder of this paper, for the publication and distribution of this paper as part of the ICAS proceedings or as individual off-prints from the proceedings.

7. Nomenclature

- A area (m^2)
- B empirical coefficient
- c seal clearance (m)

Fast Prediction Method for Radial Growth of Labyrinth

e specific internal energy (J·kg⁻¹)

E elastic modulus ($N \cdot m^{-2}$)

h specific enthalpy ($J \cdot kg^{-1}$)

H the convective heat transfer coefficient ($W \cdot m^{-2} \cdot K^{-1}$)

M the number of flow paths (branches)

n labyrinth seal teeth number

N and the number of convective heat transfer zones

p pressure (N·m⁻²)
P power (J·s⁻¹)
Q heat flux (J·s⁻¹)
r radius (m)

R the gas constant $(J \cdot mol^{-1} \cdot K^{-1})$

t time (s)

T temperature (K) u deformation (m) V volume (m³) W mass flow (kg·s⁻¹)

8. Greek letters

α linear expansion coefficient

δ deviation value (m)

Δ variation

v Poisson's ratio

π ratio of circumference to diameter

ρ density (kg·m³)

 ω angular velocity (rad·s⁻¹)

9. Subscripts

0 Initial parameter

col cold air

exp experiment data

env environmental parameter

hot hot air

i the i-th branch in inlet parameter

j the j-th heat transfer zone

lab labyrinth parameter out outlet parameter rotor parameter

r1 thermal deformation of rotor r2 centrifugal deformation of rotor

s stator parameter

thermal deformation of statorpressure deformation of stator

v chamber parameter

win window power

10. Superscripts

Stagnation Parameter

11. Author Email Address

Chuankai Liu: liuchuankai@buaa.edu.cn Tel: +86 13488824121

Or Zijun Li: lizijun@buaa.edu.cn Tel: +86 13920737316

12. References

- [1] ZHANG Zai-de. Analysis and Verification of Turboshaft Engine Air Parking Fault. *Aeroengine*, Vol.45, No.4 pp 62-65, 2019 (in Chinese)
- [2] ZOU Mi, Ma Jian-dong, LIANG jin-hua, et al. Failure analysis for small and reverse axial force of aeroengine. *Gas Turbine Experiment and Research*, Vol. 35, No. 1, pp 45-47,2022. (in Chinese)
- [3] Subramanian, S, Sekhar, AS, & Prasad, BVSSS. Performance Analysis of a Rotating Labyrinth Seal With Radial Growth. *Proceedings of the ASME Turbo Expo 2013: Turbine Technical Conference and Exposition*. San Antonio, Texas, USA. Vol 3C: Heat Transfer, 10, V03CT18A005, 2013.
- [4] Subramanian S, Sekhar A, Prasad B. On the choice of initial clearance and prediction of leakage flow rate for a rotating gas turbine seal. *Proceedings of the Institution of Mechanical Engineers Part C Journal of Mechanical Engineering Science*, Vol. 230, No. 10, pp 1586-1601 2015.
- [5] Subramanian S, Sekhar AS, Prasad BVSSS. Influence of combined radial location and growth on the leakage performance of a rotating labyrinth gas turbine seal. *Journal of Mechanical Science and Technology*, Vol. 29, No. 6, pp 2535-2545, 2015.
- [6] Subramanian S, Sekhar S, et al. Assessment of Analytical Predictions for Radial Growth of Rotating Labyrinth Seals. *International Journal of Turbo & Jet Engines*, Vol. 35, No. 3, pp 265-279, 2018.
- [7] Kong X , Liu G , Liu Y ,et al. Performance evaluation of the inter-stage labyrinth seal for different tooth positions in an axial compressor. *Proceedings of the Institution of Mechanical Engineers*, *Part A: Journal of Power and Energy*, Vol. 232, No. 6, pp 579-592, 2018.
- [8] Kong X , Liu G , Liu Y ,et al. Experimental testing for the influences of rotation and tip clearance on the labyrinth seal in a compressor stator well. *Aerospace science and technology*, Vol. 71, pp 556-567 2017.
- [9] Xiaozhi K , Yuxin L , Huawei L U ,et al. Performance Analysis of Inter-Stage Leakage Flows at Rotating Conditions in an Axial Compressor. *Journal of Thermal Science*, Vol. 29, No. 6, pp 1558-1568, 2020.
- [10] Valencia A G , Dixon J A , Guardini A ,et al. Heat Transfer in Turbine Hub Cavities Adjacent to the Main Gas Path Including FE-CFD Coupled Thermal Analysis. *Proceedings of the ASME 2011 Turbo Expo: Turbine Technical Conference and Exposition*, Vancouver, British Columbia, Canada, Vol 5: Heat Transfer, Parts A and B, 11, pp 833-843, 2011.
- [11] Hannes Lück, Schfer M, Schiffer H P. Simulation of Thermal Fluid-Structure Interaction in Blade-Disk Configuration of an Aircraft Turbine Model, *Proceedings of the ASME Turbo Expo 2014: Turbine Technical Conference and Exposition*, Düsseldorf, Germany, Vol 5A: Heat Transfer, 13, V05AT11A014, 2014
- [12] Amirante D., Hills N. J., Barnes C. J. Thermo-Mechanical Finite Element Analysis/Computational Fluid Dynamics Coupling of an Interstage Seal Cavity Using Torsional Spring Analogy. *Journal of Turbomachinery*, Vol. 134, No. 5, pp 1-9, 2012.
- [13] Amirante D., Hills N. J., Barnes C. J. A Moving Mesh Algorithm for Aero-Thermo-Mechanical Modelling in Turbomachinery. *International Journal for Numerical Methods in Fluids*, Vol. 70, No. 9, pp 1118-1138, 2012.
- [14] Amirante D., Hills N. J., Barnes C. J. Use of Dynamic Meshes for Transient Metal Temperature Prediction. *Proceedings of the ASME Turbo Expo 2012: Turbine Technical Conference and Exposition.* Copenhagen, Denmark: International Gas Turbine Institute, Vol. 4, 12, pp 2073-2084, 2012.
- [15] Tondello G., Boruszewski W., Mengele F., et al. Coupled Simulation of the Secondary Air Flow, Heat Transfer, and Structural Deflection of a Gas Turbine Engine. *Proceedings of the ASME Turbo Expo 2012: Turbine Technical Conference and Exposition.* Copenhagen, Denmark: International Gas Turbine Institute, Vol. 4, 9, pp 2295-2303, 2012.
- [16] Ganine V., Hills N., Miller M., et al. Implicit Heterogeneous 1D/2D Coupling for Aero-Thermo-Mechanical Simulation of Secondary Air Systems. *Proceedings of the ASME Turbo Expo 2015: Turbine Technical Conference and Exposition*. Montreal, Quebec, Canada: International Gas Turbine Institute, Vol. 5C, 10, V05CT15A022, 2015.
- [17] Giuntini S., Andreini A., Facchini B. Finite Element Transient Modelling for Aero-Thermo-Mechanical

Fast Prediction Method for Radial Growth of Labyrinth

Analysis of Whole Gas Turbine Engine. Proceedings of the *ASME Turbo Expo 2019: Turbomachinery Technical Conference and Exposition.* Phoenix, Arizona, USA, Vol. 5A: Heat Transfer, V05AT20A003, 2019.

- [18] Liu C K , Liu H M , Li Y R ,et al. Modularized simulation modeling of air system with fast transients. *Journal of Aerospace Power*, Vol. 30, No. 8, pp 1826-1833, 2015. (in Chinese)
- [19] Karl Trutnovsky, Berührungsfreie Dichtungen. 1st edition, China Machine Press, 1986.
- [20] Timoshenko, Stephen P. et al. Theory of Elasticity. 3rd edition, Journal of Applied Mechanics, 1970.